JACS
JOURNAL OF THE AMERICAN CHEMICAL SOCIETY
Article
pubs.acs.org/JACS

Peptide-Bridged Dinuclear Ru(II) Complex for Mitochondrial Targeted Monitoring of Dynamic Changes to Oxygen Concentration and ROS Generation in Live Mammalian Cells

Aaron Martin, Aisling Byrne, Christopher S. Burke, Robert J. Forster, and Tia E. Keyes*

†School of Chemical Sciences, National Biophotonics and Imaging Platform, Dublin City University, Dublin 9, Ireland

Supporting Information

ABSTRACT: A novel mitochondrial localizing ruthenium(II) peptide conjugate capable of monitoring dynamic changes in local O_2 concentrations within living cells is presented. The complex is comprised of luminescent dinuclear ruthenium(II) polypyridyl complex bridged across a single mitochondrial penetrating peptide, FrFKFrFK-$CONH_2$ (r = D-arginine). The membrane permeability and selective uptake of the peptide conjugate at the mitochondria of mammalian cells was demonstrated using confocal microscopy. Dye co-localization studies confirmed very precise localization and preconcentration of the probe at the mitochondria. This precision permitted collection of luminescent lifetime images of the probe, without the need for co-localizing dye and permitted semiquantitative determination of oxygen concentration at the mitochondria using calibration curves collected at 37 °C for the peptide conjugate in PBS buffer. Using Antimycin A the ability of the probe to respond dynamically to changing O_2 concentrations within live HeLa cells was demonstrated. Furthermore, based on lifetime data it was evident that the probe also responds to elevated reactive oxygen species (ROS) levels within the mitochondria, where the greater quenching capacity of these species led to luminescent lifetimes of the probe at longer Antimycin A incubation times which lay outside of the O_2 concentration range. Although both the dinuclear complex and a mononuclear analogue conjugated to an octaarginine peptide sequence exhibited some cytotoxicity over 24 h, cells were tolerant of the probes over periods of 4 to 6 h which facilitated imaging. These metal-peptide conjugated probes offer a valuable opportunity for following dynamic changes to mitochondrial function which should be of use across domains in which the metabolic activity of live cells are of interest from molecular biology and drug discovery.

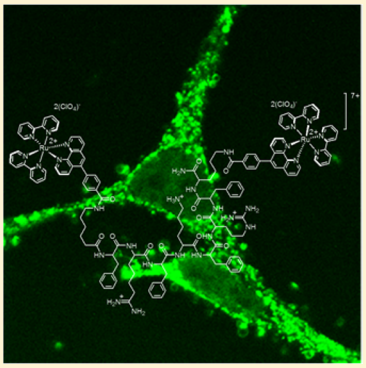

INTRODUCTION

Oxygen concentration within living cells and tissue is an important marker of metabolic status. Intracellular O_2 is the key metabolite and energy source in mammalian cells and is also a substrate for numerous enzymatic reactions which are vital for normal cell function. There are relatively few reliable ways to quantitatively measure oxygen or oxygen species within cells and fewer again capable of measuring such species at an organelle specific level. Oxygen electrodes remain a key means of measuring O_2 in tissue and cell culture medium and although quantitative, such electrodes are invasive and not suited to cells.[1] Although experiments are conducted using O_2 sensing electrodes on individual organelles, they typically must be extracted from the cell, reducing biorelevance.[2] Electron paramagnetic resonance (EPR) is suitable for both cells and tissues but is highly specialized.[3] Luminescence is currently the method of choice in cells as it is the most practical approach. O_2 is typically detected through its quenching of the excited state of the given luminophore, reducing its emission intensity and lifetime.[4,5] However, as luminescence intensity is affected by probe concentration it is a parameter unsuited to quantitative oxygen measurement. Therefore most luminescence-based assays must rely on ratiometric approaches or measurement of the luminescence lifetime of the probe.[6]

Both because triplet states tend to be long-lived and because O_2 is triplet in the ground state, most efficient quenching is achieved via energy transfer to a triplet excited state acceptor. The main probes reported for in-cell O_2 sensing have therefore been phospors. Typically these have been metal complexes or organic triplet state emitters such as porphyrins, both molecular and particle based.[7−13] However, there are relatively few probes that have been demonstrated to respond to changing oxygen concentration in a quantitative way and which are also capable of being transported across the cell membrane, without the need for permeablisation e.g. through the use of DMSO, ethanol or detergent in the media.[14,15] Our group have focused on the application of Ru(II) polypyridyl complexes for in-cell sensing, including, O_2, membrane and protein binding.[16−18] The key advantages of the Ru(II) polypyridyl probes are their photostability, oxygen sensitivity and redox and optical/photophysical tuneability. Their emission is formally a phosphorescence, from a ^{3}MLCT excited state which is populated with unity efficiency from the associated singlet absorbance.[19] This is one of their key advantages over organic probes which usually also deactivate through fluorescence and

Received: August 6, 2014
Published: September 29, 2014

   dx.doi.org/10.1021/ja508043q | J. Am. Chem. Soc. 2014, 136, 15300−15309

Scheme 1. Synthesis of Novel 5-Phenanthroline Benzoic Acid (3) and Its Ru(II) Complex Followed by Conjugation to a Mitochondrial Penetrating Peptide[a]

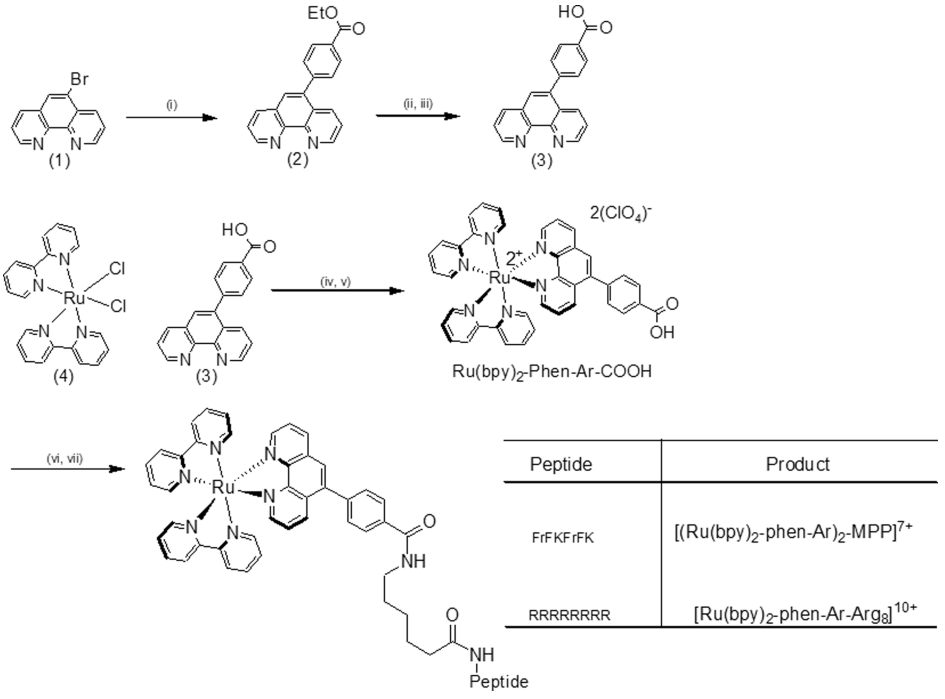

[a](i) 4-Ethoxyphenylboronic acid, K_2CO_3, Pd(dppf)Cl_2·DCM, dioxane/H_2O (3:1), 6 h, 70%. (ii, iii) DCM/MeOH (9:1), NaOH; HCl. (iv, v) EtOH/H_2O (1:1), $LiClO_{4\ (aq)}$. (vi, vii) NH_2-AHX-peptide HATU, DIPEA; $LiClO_{4\ (aq)}$.

tend, without metal coordination, at room temperature to have low quantum yields of phosphorescence. Although aqueous solubility of metal polypyridyl complexes depends on ligands and counterion identity, relatively lipophilic complexes can be rendered water-soluble by conjugation to peptides, PEGylation, and other biocompatible functional groups.[20−22] Although most reports of in-cell O_2 sensing have focused on probes in the cytoplasm, there is a strong need for probes which can be selectively directed to the organelles. Probes which distribute throughout cytoplasm along with various organelles are not very suitable as it is difficult, particularly in lifetime imaging, to identify the target organelle against the broader background of luminophore emission. In such a situation there is a requirement, for example, for a co-localization probe to identify the region of interest. By using a probe capable of accumulating in the organelle of choice, the need for such a co-localizing probe can be avoided. This is important, as in sensing such dye co-localization can lead to unwanted cross-talk such as coabsorption of the same wavelength or quenching. The key challenges therefore, are to direct probes predictably to target key organelles so that O_2 can be monitored in real time at precise organelle locations, without the need for destructive permeablization of the cell/organelle and without requirement for co-localizing probe to precisely identify the organelle against background probe emission.[23] Mitochondria are one of the key targets for O_2 sensing as they are the centers of oxygen metabolism in the cell. There, oxygen is consumed by cytochrome oxidase leading ultimately to ATP production. O_2 concentrations in this organelle directly reflect the health of the cell. Furthermore, the role of mitochondria across a wide range of debilitating diseases from cancer and diabetes to neurological disorders such as Alzheimer's, and, Multiple Sclerosis is being increasingly recognized.[24,25] Understanding O_2 concentration changes and the production of reactive oxygen species within the mitochondria in real time can therefore provide key insights into disease progression, cell death and the influence of therapy on cellular metabolism.[26,27] This organelle is also a prime target in the treatment of multiple disease states.[28]

The key challenge to directing a probe to the mitochondria, which has arisen in drug delivery, is the relatively impervious nature of the hydrophobic inner membrane. Theoretical and experimental studies have revealed that for optimal mitochondrial penetration a combination of lipophilicity and multicationic charge is required.[29] However, the relationship between chemical structure and entry remains somewhat ill-defined.[30,31]

There have been a number of examples of luminescent platinum group metal luminophores which have been reported to reach the mitochondria through manipulation of the complex structure and their appendages.,[32−34] For example, Barton et al. reported a systematic study of the effect of changing the lipophilicity of rhodium-based metallo-DNA inserters to target DNA in nucleus or mitochondria selectively in mammalian cells.[23] Lo et al., recently described a family of PEGylated cyclometalated Iridium complexes, these phosphorescent materials reached the mitochondria and exhibited strong photocytoxocity.[35] There have been a small number of reports on dinuclear ruthenium complexes applied to live cells studies, both imaging and cytotoxity.[36−38] Thomas et al. recently reported on dinculear probes as in-cell sensors for DNA detection-based on two photon luminescent lifetime imaging.[39] In a very recent study reported by Keene et al., on dinuclear ruthenium complexes bridged by *n*-alkyl chains showed cellular uptake into L1210 murine leukemia cells.[34] This demonstrated for the first time selective uptake of a dinuclear complex where

dx.doi.org/10.1021/ja508043q | J. Am. Chem. Soc. 2014, 136, 15300−15309

it was found to preferentially locate within the mitochondria. These dinuclear complexes were found to be cytotoxic.

In parallel we have been developing a targeted binuclear probe which is bridged across a mitochondrial penetrating peptide (MPP) with the aim of intramitochondrial oxygen sensing. An overarching objective of our work is to exploit peptides for truly predictable organelle targeting of the metal complex for in-cell sensing. The peptide sequence we used, FrFKFrFK-$CONH_2$, was reported previously by Kelley et al. to drive organic fluorophores to the mitochondria,[30] and we demonstrate here that this peptide also possesses the physiochemical properties needed to selectively translocate a dinuclear Ru(II) polypyridyl complex to the mitochondria, without the need for use of solvent or other membrane permeablization. Across the previous luminescent metal polypyridyl complexes which have reached the mitochondria, there have to our knowledge been no examples of their application in O_2 sensing. We report here on the first example of a Ru(II) complex to report on O_2 in the mitochondria and demonstrate using Antimycin A as a mitochondrial inhibitor, that the probe responds dynamically to O_2 concentration changes and also, it seems, to production of reactive oxygen species (ROS). This targeted binuclear complex is potentially of significant value across applications in cell biology and drug discovery where understanding the metabolic status of the mitochondria is required. This work further supports growing evidence that peptides are a truly powerful approach to achieving predictable cell permeability and organelle targeting of metal complexes for in-cell sensing.

RESULTS AND DISCUSSION

Syntheses and Characterization of Ligands and Complexes. The synthesis of 5-bromo-1,10-phenanthroline (**1**) was achieved by modification of a procedure developed by Eisenberg et al.[40] A high-pressure sealed reaction vessel containing 1,10-phenanthroline, bromine, and fuming sulfuric acid was heated at 135 °C for 23 h. Following this a Suzuki–Miyaura protocol was implemented so as to isolate ethyl 4-(1,10-phenanthrolin-6-yl) benzoate (**2**). The conditions used combined (**1**) with 4-ethoxyphenylboronic acid (1.5 equiv) and $Pd(dppf)Cl_2$. DCM (10 mol %) as catalyst and K_2CO_3 (2 equiv) as a base in dioxane:H_2O (3:1) heated to reflux for ca. 6 h (Scheme 1). This gave ethyl 4-(1,10-phenanthrolin-6-yl) benzoate (**2**) in a 70% yield.

Typically, this reaction came to completion with minimal byproducts in solution (confirmed by TLC). The desired product was isolated by flash column chromatography (DCM/MeOH 95:5) as a yellow oil which was solidified via trituration from hot $CHCl_3$ with cold pentane followed by co-solvent recrystallization from MeCN/H_2O (1:1) to yield a white powder. Base catalyzed hydrolysis of the ethyl ester functionality yielded (**3**) as outlined in Scheme 1.[41] The identity of **3** was confirmed by high-resolution positive ion mass spectrometry which revealed an m/z 301.0988, which corresponded to the peak [M + H] (calculated for $[M]^+$, m/z 300.0977).

The ligand was coordinated to cis-$Ru(bpy)_2Cl_2$ (**4**) in mixed solvent H_2O/EtOH (1:1 v/v), to yield compound $[Ru(bpy)_2$phen-Ar-$COOH]^{2+}$ $2(ClO_4)_2$ as a bright orange solid in a 79% yield.

An amide coupling protocol was employed to conjugate the parent complex to the peptide by reacting $[Ru(bpy)_2$phen-Ar-$COOH]^{2+}$ with NH_2-AHX-FrFKFrFK-$CONH_2$ (AHX = aminohexanoic acid) in the presence of HATU (1-[bis-(dimethylamino)methylene]-1H-1,2,3-triazolo[4,5-*b*]-pyridinium 3-oxid hexafluorophosphate) and DIPEA (diisopropylethylamine) in DMF.

Following the reaction, the solution was placed on ice, and a saturated aqueous solution of $LiClO_4$ was added until a bright orange precipitate formed which was filtered and washed with H_2O. The product was then dissolved in EtOH/H_2O 1:1 v/v and the EtOH removed *in vacuo*. The remaining H_2O was removed by lyophilization to yield the pure dimeric conjugate (HPLC, Figure S24). ^1H NMR analysis of the conjugate confirmed the conjugate contained two $Ru(bpy)_2$phen-Ar moieties. Single mass analysis showed the molecular weight was 2975.8765 which corresponded to the calculated mass of 2975.8643 g/mol for $C_{144}H_{150}Cl_3N_{30}O_{23}Ru_2$-$ClO_4$. ^1H NMR nuclear Overhauser effect spectroscopy (NOESY) was used to determine the conjugation points of the complex to the peptide. In order to determine which branched amine group the second ruthenium moiety was coupled to, we studied the aromatic signals on the phenylalanines. They are in close proximity to all but one of the remaining free NH_2 groups within the sequence. From NOESY, no positive contacts to any other aromatic signals associated with the coordinating ligands around the ruthenium center were observed (Figure S16). Therefore, we can conclude that the attachment must be via the least sterically hindered free amine on the terminal lysine unit (Scheme 2). The complexes and the conjugate were both prepared as perchlorate salts, and both showed excellent water solubility.

Scheme 2. Schematic of the Structure of Mitochondrial Localizing Conjugate $[(Ru(bpy)_2$phen-Ar$)_2$-MPP$]^{7+}\cdot 4(ClO_4)^-$

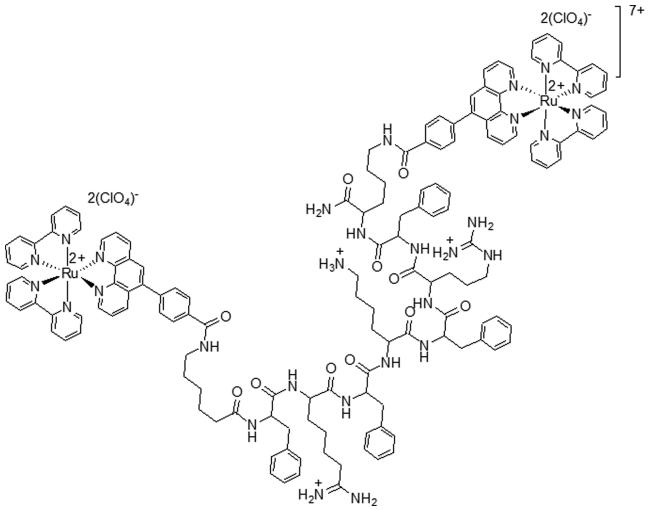

An analogous coupling protocol was used to conjugate a simple cell penetrating peptide to $[Ru(bpy)_2$phen-Ar-$COOH]^{2+}$ by reacting the complex with NH_2-AHX-$RRRRRRRR$-$CONH_2$ to yield $[Ru(bpy)_2$phen-Ar-$Arg_8]^{10+}$. The octarginine polypeptide sequence has been shown to be effective in transporting Ru(II) complexes across the cell membrane into cytoplasmic regions with nuclear exclusion without organelle specificity and was therefore used here to compare uptake and targeting ability of the peptide.[16]

Spectroscopic Properties. Figure 1 shows the absorbance and emission spectra of the ruthenium parent complex

dx.doi.org/10.1021/ja508043q | J. Am. Chem. Soc. 2014, 136, 15300–15309

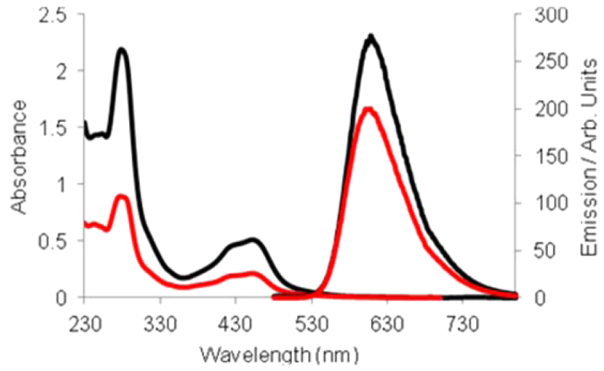

Figure 1. Absorbance and emission spectra of $[Ru(bpy)_2phen\text{-}Ar\text{-}COOH]^{2+}$ (red line) and $[(Ru(bpy)_2phen\text{-}Ar)_2\text{-}MPP]^{7+}$ (black line), respectively. Spectra were recorded at 25 μM (PBS) with emission slit widths of 5 nm and emission excitation wavelength of 460 nm.

$[Ru(bpy)_2phen\text{-}Ar\text{-}COOH]^{2+}$ and $[(Ru(bpy)_2phen\text{-}Ar)_2\text{-}MPP]^{7+}$, both in PBS solution (pH 7.4). The electronic absorption spectra for each compound show an absorption band at 460 nm ($\varepsilon \sim 17 \times 10^3$ and 41×10^3 L mol^{-1} cm^{-1} respectively) assigned to a metal to ligand charge transfer (MLCT) transition. The larger molar absorptivity for $[(Ru(bpy)_2phen\text{-}Ar)_2\text{-}MPP]^{7+}$ is attributed to the presence of two ruthenium centers at the peptide bridge. The conjugate, $[Ru(bpy)_2phen\text{-}Ar\text{-}Arg_8]^{10+}$, also displays a band at 460 nm but with a similar ε (19×10^3 L mol^{-1} cm^{-1}) to that of the parent presursor. When excited into the MLCT absorbance, an intense emission band for $[Ru(bpy)_2phen\text{-}Ar\text{-}COOH]^{2+}$ was observed centered around 604 nm with a quantum yield of 0.046 ± 0.003 which is slightly lower than that of the peptide bound species [Φ = 0.056 ± 0.002 for $[(Ru(bpy)_2phen\text{-}Ar)_2\text{-}MPP]^{7+}$ and 0.067 ± 0.005 for $[Ru(bpy)_2phen\text{-}Ar\text{-}R_8]^{10+}$.

Under aerated conditions, $[Ru(bpy)_2phen\text{-}Ar\text{-}COOH]^{2+}$ exhibits a lifetime of 455 ± 11 ns in aqueous PBS buffer which is increased to 780 ± 9 ns after deaeration by N_2 at room temperature.

Temperature-Dependent Response of $[(Ru(bpy)_2phen\text{-}Ar)_2\text{-}MPP]^{7+}$ Luminescence to Oxygen Concentration. The response of $[(Ru(bpy)_2phen\text{-}Ar)_2\text{-}MPP]^{7+}$ to O_2 concentration was explored by examining the emission intensity of this complex with varying $[O_2]$ in PBS buffer. The O_2 concentration of each solution was measured independently using a Presense fiber optic O_2 probe which recorded saturation O_2 concentration in PBS buffer (pH 7.4) as 220 μM. The emission spectrum was recorded at O_2 saturation, and a 3 mL solution was then deaerated under N_2 for 15 min, wherein a 0 μM concentration of O_2 was recorded within the sample. As expected there was an increase in emission intensity (Figure S38). The solution was gradually reaerated, the O_2 concentration recorded by fiber optic probe, and the emission spectra and lifetime collected from $[(Ru(bpy)_2phen\text{-}Ar)_2\text{-}MPP]^{7+}$ as a function of O_2 concentration to yield the linear Stern–Volmer plot (eq 1, Figure S39).

Figure 2B shows the Stern–Volmer plots of luminescent lifetime versus O_2 concentration for $[(Ru(bpy)_2phen\text{-}Ar)_2\text{-}MPP]^{7+}$ by O_2 at 18 °C (as for the *I* Figure 2A) and also at 37 °C. It is important to note the temperature sensitivity of the Stern–Volmer plot. Ruthenium polypyridyl complexes typically exhibit temperature-dependent luminescence, with decreases in quantum yield and lifetime commonly observed with increasing temperature. This behavior is attributed to the population of a

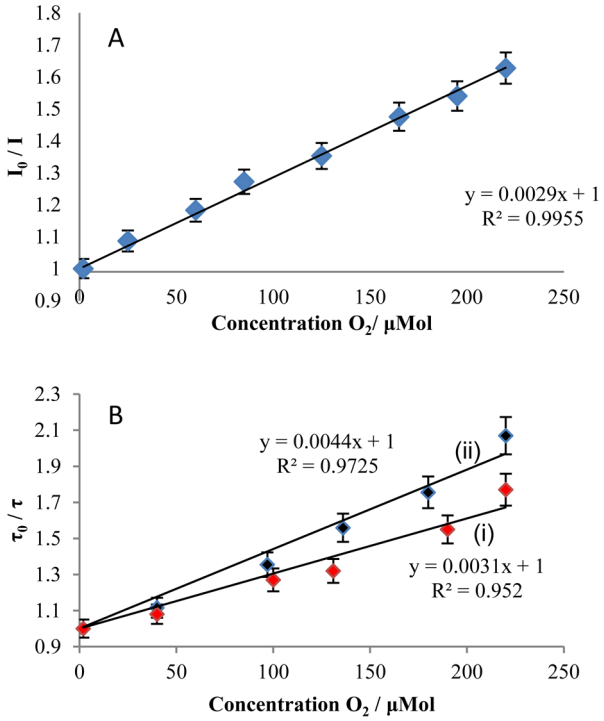

Figure 2. Stern–Volmer plots for quenching of $[(Ru(bpy)_2phen\text{-}Ar)_2\text{-}MPP]^{7+}$ by molecular oxygen. (A) Emission intensity versus $[O_2]$ from saturation to deaeration. Stern–Volmer plot of emission intensity as a function of $[O_2]$ at 18 °C. (B) Stern–Volmer plot of emission lifetime as a function of $[O_2]$ at (i) 18 °C and (ii) 37 °C.

thermally accessible triplet metal centered ^{3}eg* state which is promoted from the ^{3}MLCT state in Ru(II) complexes containing polypyridyl ligands, though it can be alleviated by the introduction of strong σ-donating ligands.[42,43] As an example of the sensitivity of the photophysical properties of $[(Ru(bpy)_2phen\text{-}Ar)_2\text{-}MPP]^{7+}$, the emission lifetime is 698 ± 6 ns in aerated PBS and 1.23 μs ± 10 ns in deaerated PBS at room temperature (18 °C), whereas at 37 °C, in aerated media, the lifetime $[(Ru(bpy)_2phen\text{-}Ar)_2\text{-}MPP]^{7+}$ was substantially lower at 458 ± 7 ns in aerated and 948 ± 6 ns in deaerated media. Comparison of the intensity and lifetime based Stern–Volmer plots at room temperature confirms K_{SV} (the slope) is the same in each case, consistent with dynamic quenching. From K_{SV} and the lifetime values in the absence of O_2, we obtain oxygen quenching rate constants, k_q, of 2.5×10^9 M s^{-1} and 4.64×10^9 M s^{-1} for 18 and 37 °C, respectively. The latter value is slightly lower than, but consistent with, the O_2 quenching rate reported by Demas et al. (3.2×10^9 M s^{-1}) at 20 °C for O_2 quenching of $[Ru(bpy)_3]^{2+}$.[44] The somewhat lower O_2 sensitivity seen here may be attributed to lower access of O_2 to the complex because of the bulky peptide as noted previously.[18] From the 37 °C plot we now have a calibration curve from which we can estimate O_2 concentration within the cell from fluorescence lifetime imaging.

Cell Uptake and Mitochondrial Staining. The uptake of $[Ru(bpy)_2phen\text{-}Ar\text{-}COOH]^{2+}$ and $[(Ru(bpy)_2phen\text{-}Ar)_2\text{-}MPP]^{7+}$ by HeLa and CHO cells were compared across a range of dye concentrations (10–100 μM) in PBS buffer. Both cell lines failed to take up the parent precursor across any of these concentrations. Such poor cellular penetrability by ruthenium complexes, in the absence of permeablization, e.g., with organic solvent has been noted previously.[45] In contrast

dx.doi.org/10.1021/ja508043q | J. Am. Chem. Soc. 2014, 136, 15300–15309

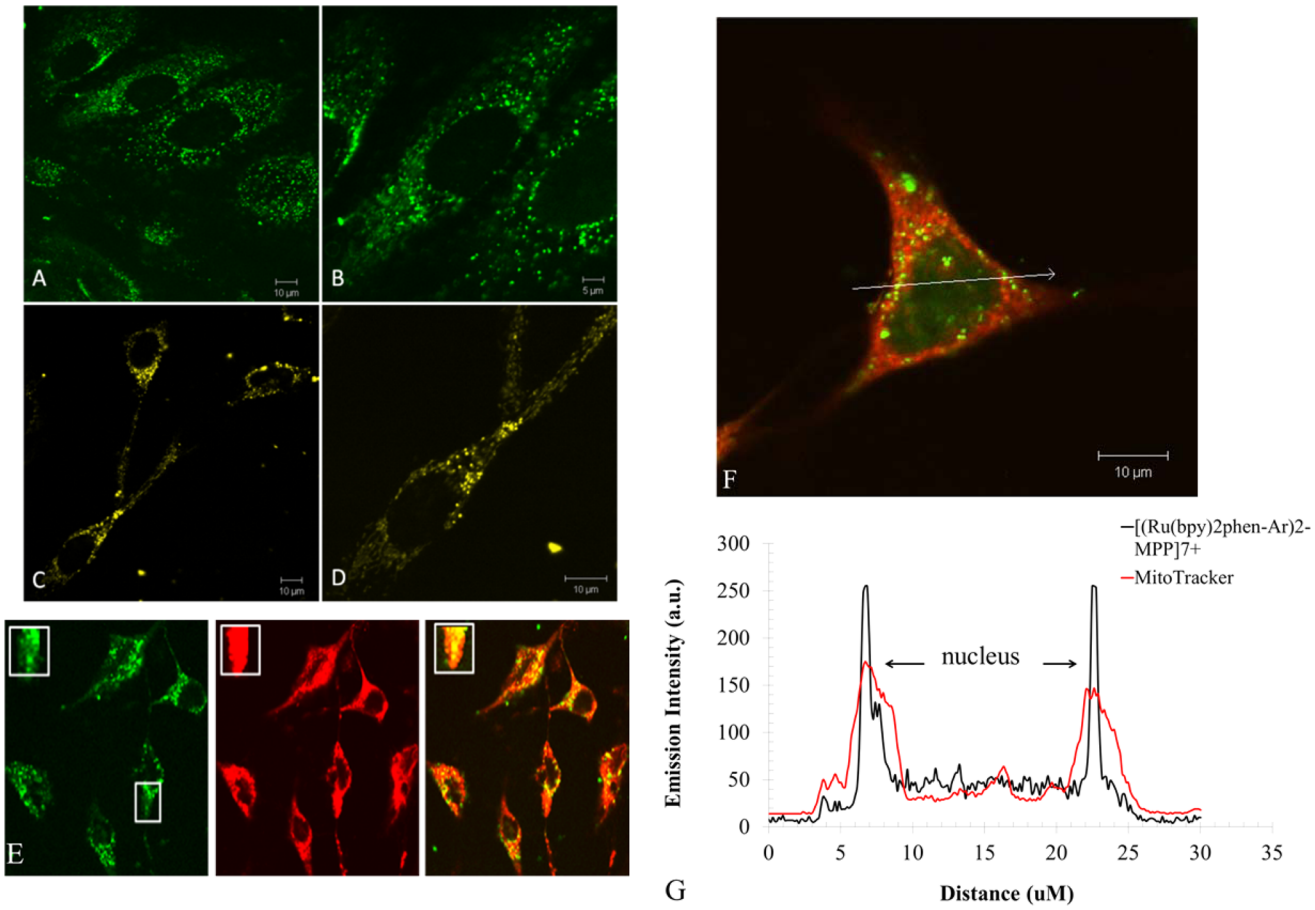

Figure 3. (A,B) Confocal luminescence Imaging of $[(Ru(bpy)_2phen\text{-}Ar)_2\text{-}MPP]^{7+}$ in HeLa cells. (C,D) Confocal luminescence Images of $[Ru(bpy)_2phen\text{-}Ar\text{-}Arg_8]^{10+}$ in HeLa cells. (E) Co-localization studies were carried out using 500 nM of the mitochondrial marker MitoTracker Deep Red. Cells were treated with $[(Ru(bpy)_2phen\text{-}Ar)_2\text{-}MPP]^{7+}$for 2 h and MitoTracker Deep Red for 30 min. $[(Ru(bpy)_2phen\text{-}Ar)_2\text{-}MPP]^{7+}$ is shown in green, $[(Ru(bpy)_2phen\text{-}Ar)_2\text{-}MPP]^{7+}$ in red, and co-stained regions are shown in yellow on the left. (F) Cross-section image describing the co-localization of $[(Ru(bpy)_2phen\text{-}Ar)_2\text{-}MPP]^{7+}$ and MitoTracker Deep Red in HeLa cell shown in green, and its corresponding plot (G) demonstrating both compounds localize within the mitochondria and are nuclear excluding. $[(Ru(bpy)_2phen\text{-}Ar)_2\text{-}MPP]^{7+}$ was excited using 488 nm argon laser and emission collected using long pass 630 nm filter set. MitoTracker Deep Red was excited with 633 nm HeNe laser and emission collected using long pass 630 nm filter (G); (scale bar: A, C, D, and F 10 μM; and B 5 μM).

$[(Ru(bpy)_2phen\text{-}Ar)_2\text{-}MPP]^{7+}$ was taken up rapidly and irreversibly by the cells in a concentration-dependent manner. 75 μM in the contacting solution was found to be optimum concentration for the uptake and imaging in terms of a balance between emission intensity and cytotoxicity. Interestingly, conjugate uptake was found to be temperature dependent. It was found for example that when incubated with HeLa cells at 4 °C, $[(Ru(bpy)_2phen\text{-}Ar)_2\text{-}MPP]^{7+}$ failed to cross the cell membrane. Instead, the conjugate appears to localize in the membrane even after extensive incubation (Figure S37). This result indicates that uptake is an activated process such as endocytosis.

Detailed uptake and localization studies were carried out on $[(Ru(bpy)_2phen\text{-}Ar)_2\text{-}MPP]^{7+}$ using confocal laser scanning microscopy (CLSM). The initial uptake is fast; the conjugate enters the cells within 5 min of its addition to the contacting solution (Figure S25). After an incubation period of 1 h it appeared initially to concentrate within the cytoplasm and then localizes strongly in the mitochondria, and localization is complete at 37 °C following in 2 h incubation, both in the presence and absence of light. It is evident that the dye strongly preconcentrates inside the mitochondria, although luminescence imaging shows that some complex remains within the cytoplasm, furthermore the conjugate is nuclear excluding (Figure 3A,B). Similar nuclear exclusion was observed for $[Ru(bpy)_2phen\text{-}Ar\text{-}Arg_8]^{10+}$ when incubated with HeLa cells at 75 μM for 2 h. It is strongly membrane permeable but distributes within the cytoplasm, excluding the nucleus (Figure 3C,D) and with no evidence for mitochondrial uptake. To conclusively confirm localization of $[(Ru(bpy)_2phen\text{-}Ar)_2\text{-}MPP]^{7+}$at the mitochondria, HeLa cells incubated with 75 μM of the conjugate for 2 h at 37 °C were dual stained with MitoTracker Deep Red. The MitoTracker showed strong co-localization with the conjugate, in Figure 3E, $[(Ru(bpy)_2phen\text{-}Ar)_2\text{-}MPP]^{7+}$ is seen in green, MitoTracker in red, and their co-localization in yellow. Figure 3F expands a single cell which clearly shows superimposed emissions of $[(Ru(bpy)_2phen\text{-}Ar)_2\text{-}MPP]^{7+}$and the MitoTracker at a single cell and confirms they are co-localized. Indeed an x-scan of emission intensity from each probe, shown in Figure 3F, indicates that both are at a coincident location and nuclear excluding.

However, it appears that $[(Ru(bpy)_2phen\text{-}Ar)_2\text{-}MPP]^{7+}$ is even more narrowly confined to the mitochondrial region than MitoTracker, suggesting perhaps that Mitotracker is more confined to the membrane region of the mitochondria than its interior.

dx.doi.org/10.1021/ja508043q | J. Am. Chem. Soc. 2014, 136, 15300−15309

This result indicates that this mitochondrial directing peptide sequence can be used to direct metal complexes to the mitochondria selectively with a much lower background concentration of the probe remaining in the cytoplasm. This is an important result as the background contributions from $[(Ru(bpy)_2phen\text{-}Ar)_2\text{-}MPP]^{7+}$ residing in cytoplasm is readily distinguished from the mitochondria making localized measurement of luminescent lifetime and therefore O_2 concentration at the mitochondria potentially relatively straightforward.

Fluorescence Lifetime Imaging and Oxygen Dependence Studies in HeLa cells. This was borne out in the fluorescence lifetime imaging experiments shown in Figure 4,

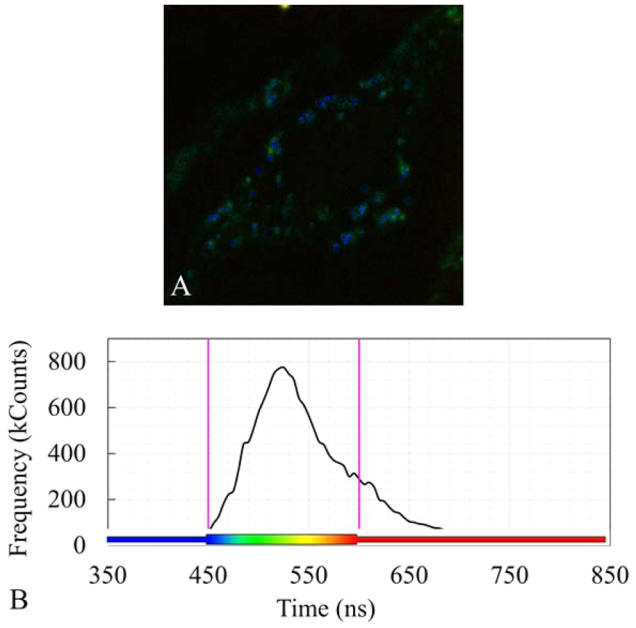

Figure 4. FLIM image (A) and its corresponding lifetime distribution (B) of $[(Ru(bpy)_2phen\text{-}Ar)_2\text{-}MPP]^{7+}$, in the mitochondria in HeLa cells. Cells were incubated with 75 μM of the conjugate in the dark for 2 h. FLIM image and lifetime were recorded exciting with 405 nm laser line and emission collected using 530 nm filter set.

left, where the mitochondria are clearly distinguished from the FLIM signal without the need for costaining. At 37 °C in aqueous, air saturated PBS solution, τ of $[(Ru(bpy)_2phen\text{-}Ar)_2\text{-}MPP]^{7+}$ was recorded as 458 ± 6 ns. Figure 4 shows the distribution of luminescent lifetimes of $[(Ru(bpy)_2phen\text{-}Ar)_2\text{-}MPP]^{7+}$ within the mitochondria of live HeLa cells. From the color distribution chart, the lifetime of the conjugate within the mitochondria appears to be 525 ± 10 ns which, based on the calibration plot at 37 °C, represents an intracellular O_2 concentration of ≈183 μM. (The surrounding solution was air saturated, confirmed by Fiber optic O_2 probe and the lifetime of the complex in this solution). The lower O_2 concentration at the mitochondria is expected for normally metabolizing cells.

Monitoring the Respiratory Responses of Cells to Mitochondrial Uncoupler Antimycin A. Such precise mitochondrial localization with O_2 quantitation has, to our knowledge, not been demonstrated previously. Others have achieved cellular penetration with an O_2 sensitive probe and realized perinuclear localization but with a broad cellular diffusion pattern including mitochondrial uptake.[14]

In order to assess if the probes could respond dynamically to changes in mitochondrial function, HeLa cells were loaded with $[(Ru(bpy)_2phen\text{-}Ar)_2\text{-}MPP]^{7+}$ and then treated with Antimycin A. Antimycin A is a product comprised of Antimycin A1 and A3 derived from *Streptomyces kitazawensis* which has been widely studied using HeLa cells.[46−49] It is a classical mitochondrial uncoupler, which predictably changes oxygen levels within the mitochondria through inhibition of electron transport between cytochromes *b* and *c* at Complex III in mitochondria. The consequences of this inhibition are an increase in O_2 concentration at the mitochondria to ambient levels as its consumption at the mitochondria is terminated and eventually an increase in ROS and decrease in ATP production.[50,51]

Here, Antimycin A was added to live HeLa cells following their incubation with $[(Ru(bpy)_2phen\text{-}Ar)_2\text{-}MPP]^{7+}$for 2 h. Using FLIM, the lifetime of the conjugate was monitored at 10 min intervals over 90 min following Antimycin administration. Examples of the FLIM images collected over this period along with the lifetime distributions of $[(Ru(bpy)_2phen\text{-}Ar)_2\text{-}MPP]^{7+}$ from the mitochondria are shown in Figure 5. Figure 6 shows a

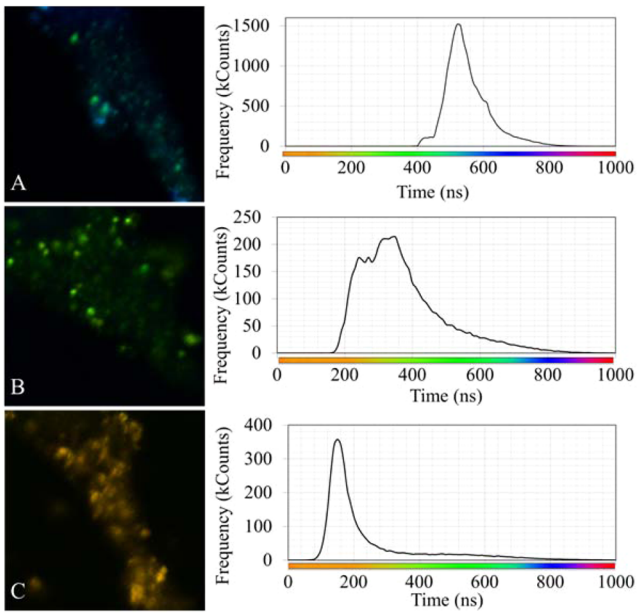

Figure 5. Luminescence lifetime distributions of $[(Ru(bpy)_2phen\text{-}Ar)_2\text{-}MPP]^{7+}$from luminescence lifetime imaging of HeLa cells in response to the addition of Antimycin A. HeLa cells were incubated with $[(Ru(bpy)_2phen\text{-}Ar)_2\text{-}MPP]^{7+}$for 2 h in the dark (A), and Antimycin A (200 μM/mL) was added. Cells were incubated for 10 min with Antimycin, and FLIM recorded (B). Cells were incubated for a further 90 min, where total exposure time was 100 min, and FLIM lifetime recorded (C) (n = 2). FLIM was carried out by accumulating photon counts over 10 min in each case under identical, wavelength, and laser intensity conditions.

plot of the luminescent lifetime from the mitochondria as a function of incubation time for HeLa cells with Antimycin A as well as a control, in which the lifetime of $[(Ru(bpy)_2phen\text{-}Ar)_2\text{-}MPP]^{7+}$ at the mitochondria over time was measured from HeLa cells without addition of Antimycin A. The control shows, within experimental error, no change in luminescent lifetime over time. The results from the Antimycin A treated cells show an initial decrease in $\tau_{average}$ from the cell mitochondria from 525 to 423 ns after 10 min incubation of the cells with Antimycin A (200 μg/mL) to the cells. This

dx.doi.org/10.1021/ja508043q | J. Am. Chem. Soc. 2014, 136, 15300−15309

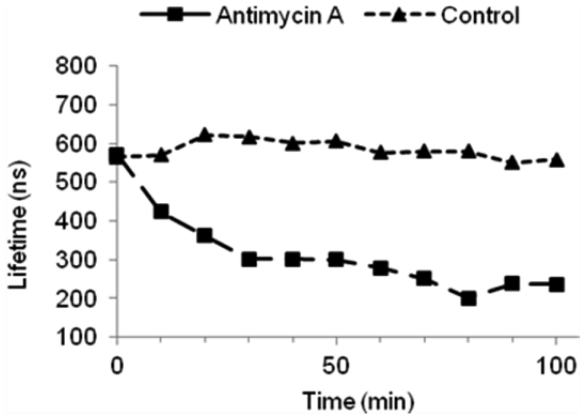

Figure 6. Effects of Antimycin A on the lifetime of $[(Ru(bpy)_2phen\text{-}Ar)_2\text{-}MPP]^{7+}$ over 100 min at 37 °C. FLIM images were acquired every 10 min following exposure of HeLa cells to the drug. The control sample of $[(Ru(bpy)_2phen\text{-}Ar)_2\text{-}MPP]^{7+}$ only was measured without any addition of mitochondrial uncoupling reagent. Sample excited using 405 nm laser and emission collected using 530 nm filter set.

decrease is indicative of O_2 diffusion from the cytoplasm/media which in the absence of O_2 consumption by Complex III returns O_2 close to saturation levels. However, this decrease in lifetime continued until a plateau was reached at approximately 228 ns ($\tau_{average}$) after 100 min (Figures 5 and 6). It is important to note that in a control experiment Antimycin A had no effect on the luminescence intensity or lifetime of $[(Ru(bpy)_2phen\text{-}Ar)_2\text{-}MPP]^{7+}$ in solution. Given the dramatic decrease in luminescent lifetime of the conjugate over extended incubation times with Antimycin A, and the fact that $[O_2]$ cannot exceed saturation, there must exist a separate quenching pathway for $[(Ru(bpy)_2phen\text{-}Ar)_2\text{-}MPP]^{7+}$. This quenching pathway is attributed to the ROS generated, induced by inhibition of mitochondrial function. Superoxide anion $O_2^{\bullet-}$, H_2O_2, and hydroxyl radical have all been shown to be increased in Antimycin A treated mitochondria.[50] All three, on the basis of their redox potentials, are expected to be capable of quenching the excited of $[(Ru(bpy)_2phen\text{-}Ar)_2\text{-}MPP]^{7+}$, although the quenching rate by hydrogen peroxide would be expected to be relatively slow.[52] It is therefore reasonable to assume that in the mitochondria in addition to responding to O_2 concentration the conjugate is also reporting on ROS generation.

Cytotoxicity and Phototoxicity. Consideration of the cytotoxicity of $[(Ru(bpy)_2phen\text{-}Ar)_2\text{-}MPP]^{7+}$ is important in assessing their suitability as O_2/ROS probes. Cytotoxicity studies were carried out using the Resazurin (Alamar Blue) assay to assess cell viability after 24 h incubation with $[Ru(bpy)_2phen\text{-}Ar\text{-}COOH]^{2+}$ and $[(Ru(bpy)_{2p}hen\text{-}Ar)_2\text{-}MPP]^{7+}$ over a concentration range of 0−200 μM. The data are shown in Figure S27. It was found that $[Ru(bpy)_2phen\text{-}Ar\text{-}COOH]^{2+}$ exhibited no cytotoxic effects on the cells, with 75% cell viability up to 200 μM. This is expected; as described above, this complex is not effective at penetrating the cell membrane, and uptake is negligible. However, viability of cells was only 15% when incubated with $[(Ru(bpy)_2phen\text{-}Ar)_2\text{-}MPP]^{7+}$, at 200 μM for 24 h. The cytotoxicity was dose dependent with 40% viability observed after 24 h at our working concentration of 75 μM (IC_{50} = 47 ± 1.1 μM). A time-dependent cytotoxicity study was carried out on $[(Ru(bpy)_2phen\text{-}Ar)_2\text{-}MPP]^{7+}$ at 75 μM over 1−7 h to assess cell viability during our working incubation time. After 5 h 40% of the cells remained viable (Figure S28).

To assess if the toxicity was specifically due to the properties of the metal complex or due to specifically to its localization within the mitochondria, $[Ru(bpy)_2phen\text{-}Ar\text{-}COOH]^{2+}$ was conjugated to a simple cell penetrating peptide (CPP) octa-arginine to produce $[Ru(bpy)_2phen\text{-}Ar\text{-}Arg_8]^{10+}$. Polyarginine peptides have been shown to deliver complexes to the cytoplasmic region of the cell, with no specific target. $[Ru(bpy)_2phen\text{-}Ar\text{-}Arg_8]^{10+}$ was incubated at varying concentrations with HeLa cells for 24 h and cell viability assessed using the Resazurin (Alamar Blue) reagent. Figure S27 shows that $[Ru(bpy)_2phen\text{-}Ar\text{-}Arg_8]^{10+}$ was cytotoxic, there was 0% cell viability at concentrations in HeLa cells incubated with concentrations of 150 and 200 μM following 24 h (IC_{50} = 44 ± 0.7 μM). This suggests that it is the parent complex which is fundamentally toxic toward the cells and not necessarily a feature of its subcellular localization. As the polyarginine delivers the complex in a nonselective manner to the cytoplasm and distributes it widely without specific preconcentration within organelles such as the endoplasmic reticulum, lysosomes, and mitochondria. (Figures 3C,D). Furthermore, the behavior of this complex contrasts strongly with the behavior of peptide conjugates of $[Ru(bpy)_2PIC]^{2+}$ complex (PIC is 2-(4-carboxyphenyl)-imidazo-[4,5-*f*][1,10]-phenanthroline). The octa-arginine conjugate of this complex showed very similar distribution to $[Ru(bpy)_2phen\text{-}Ar\text{-}Arg_8]^{10+}$ but showed low cytotoxicity.[17]

For the purposes of imaging/O_2 determination, we found that when incubated in the dark for 2 h, the cells are viable, toxicity is induced only over periods exceeding 4 h. We probed the effect of exposure of $[(Ru(bpy)_2phen\text{-}Ar)_2\text{-}MPP]^{7+}$ incubated cells to a light source to see if light induced cytotoxicity, Figure 7.

The photocytoxicity of $[(Ru(bpy)_2\ phen\text{-}Ar)_2\text{-}MPP]^{7+}$ was followed in HeLa cells by assessing the uptake of DRAQ 7 in $[(Ru(bpy)_2\ phen\text{-}Ar)_2\text{-}MPP]^{7+}$ loaded cells over time under visible irradiation, Figure 7A−D shows the results. After 20 min continuous irradiation of $[(Ru(bpy)_2phen\text{-}Ar)_2\text{-}MPP]^{7+}$ loaded cells at 488 nm we observed significant cell death, even before the complex had time to accumulate strongly within the mitochondria. This is consistent with the fundamental photocytoxicity of the complex rather than cytotoxicity associated with its localization. An area of the same sample that was not exposed to light was examined as a control, and no damage to the cells in this region was detected, indicating that the uptake of DRAQ 7, i.e., cytotoxicty was indeed induced by irradiation, (Figure 7E,F). Further control experiments show the cells are still viable at the scanning intensities used during illumination in the absence of dye. No DRAQ 7 entered the cells up to and after 50 min of scanning (Figure S26). This confirmed that the cell death is due to the presence of $[(Ru(bpy)_2phen\text{-}Ar)_2\text{-}MPP]^{7+}$.

As $[(Ru(bpy)_2phen\text{-}Ar)_2\text{-}MPP]^{7+}$ is not toxic to the cells when incubated for 2 h in the dark, we were interested to assess if phototoxicity was even greater when the dye had accumlated in the mitochondria. HeLa cells were incubated with $[(Ru(bpy)_2phen\text{-}Ar)_2\text{-}MPP]^{7+}$ (75 μM) for 2 h in the dark and then exposed to light source. The cells were continuously irradiated at 488 nm under 0.64 $\mu W/cm^{-3}$ laser power. Cellular toxicity under these conditions was evident after 20 min exposure time (Figure 7E,F), which is comparable to the time taken for photocytoxicity before the dye reached the mitochondria. Again, the photodamage was only observed in the areas exposed to light. This was similar to the effects seen during

dx.doi.org/10.1021/ja508043q | J. Am. Chem. Soc. 2014, 136, 15300−15309

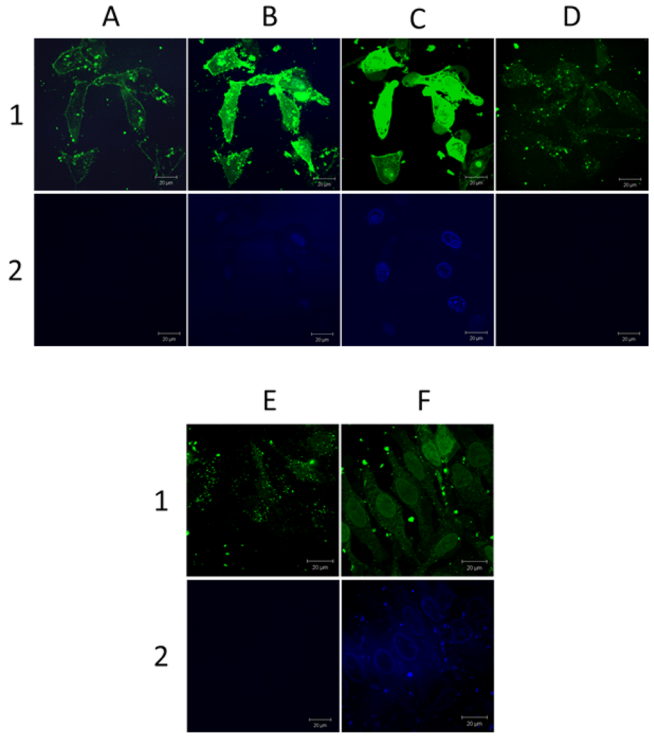

Figure 7. Phototoxicity of $[(Ru(bpy)_2phen\text{-}Ar)_2\text{-}MPP]^{7+}$ in HeLa cells. In both experiments, row 1 shows both channels for $[(Ru(bpy)_2phen\text{-}Ar)_2\text{-}MPP]^{7+}$and DRAQ 7, and row 2 shows the DRAQ 7 channel only to record toxicity (scale bar 20 μM). Immediate uptake of $[Ru(bpy)_2phen\text{-}Ar]_2\text{-}MPP^{7+}$ is evident in images collected after 5 min exposure in (A), but no toxicity to cells is observed. After 20 min some toxicity is seen (B), and after 25 min DRAQ 7 has entered the nucleus of all the cells indicating cell death (C). After 35 min of exposure to $[Ru(bpy)_2phen\text{-}Ar]_2\text{-}MPP^{7+}$ in a new location of the same sample that has not been exposed to the laser no entry of DRAQ 7 observed (D). Lastly, HeLa cells were incubated with 75 μM $[(Ru(bpy)_2phen\text{-}Ar)_2\text{-}MPP]^{7+}$for 2 h in the dark, washed, and DRAQ 7 added (E). Cells were exposed to continuous irradiation and DRAQ 7 entered the nucleus after 20 min scanning (F). Laser power used was 0.64 $\mu W/cm^{-3}$.

uptake phototoxicity studies prior to probe localization. As the cells were viable for up to 7 h of incubation in the dark (Figure S28), these results suggest that $[(Ru(bpy)_2phen\text{-}Ar)_2\text{-}MPP]^{7+}$ is photocytotoxic. Furthermore, it is evident that $[(Ru(bpy)_2phen\text{-}Ar)_2\text{-}MPP]^{7+}$ does not need to be located within the mitochondria to induce photo damage upon the cells. Interestingly luminescence from $[(Ru(bpy)_2phen\text{-}Ar)_2\text{-}MPP]^{7+}$ showed a 3-fold emission intensity increase upon photodamage to the cell. Likewise, after illumination on live uptake, phototoxicity toward the cell resulted in a 5-fold increase in emission intensity of $[(Ru(bpy)_2phen\text{-}Ar)_2\text{-}MPP]^{7+}$ from within the cell. This is compared to the intensity when incubated without light exposure. A similar effect was noted for $[Ru(phen)_3]^{2+}$, which when illuminated in live cells caused cell death.[22] Similarly an increase in luminescence intensity was also recorded after the complex induced photo damage to the cells.

It is important to note that although the photocytotoxicty of the complexes represents an issue for conventional confocal imaging, FLIM uses low energy, pulsed irradiation, and so photocytotoxity is not a significant issue in such measurements.

CONCLUSIONS

A luminescent dinuclear ruthenium(II) probe bridged across a mitochondrial penetrating peptide sequence, FrFKFrFK, exhibited excellent cell permeability with rapid, irreversible uptake, and accumulation in test cells in common growth media over approximately 20 min. The complex concentrates very precisely inside the mitochondria over a 2 h period. This was confirmed from colocalisation studies which showed that the complex was strongly confined to the mitochondria with much weaker staining of the remainder of the cell and exclusion from the nucleus.

The probe responds dynamically to changes in O_2 concentration as demonstrated by a series of *in vitro* calibration studies of both emission intensity and lifetime versus $[O_2]$ (μM) at 18 °C and at 37 °C. As expected for ruthenium complexes with modestly σ donating ligands, the calibration curves were temperature sensitive. The ability of the probes to respond to O_2 changes within the mitochondria of live HeLa cells was explored by artificially altering the metabolic state of the cells using a classical mitochondrial uncoupling reagent, Antimycin A, and assessing the lifetime profile of the probe within the mitocondria using fluorescence lifetime imaging.

$[(Ru(bpy)_2phen\text{-}Ar)_2\text{-}MPP]^{7+}$ responded rapidly to changing O_2 concentration, and after 10 min exposure to Antimycin A the $[O_2]$ returned to what seemed to be air saturated levels. Further incubation to a 100 min exposure time led to τ of 228 ns, which is shorter than the luminescence lifetime in air saturated solution. This indicates that the complex is being quenched by ROS generated from the action of the Antimycin A.

The complexes were moderately cytotoxic in the dark, and under conditions used for imaging they remained more than 40% viable over 24 h. However, under continuous photoirradiation at 488 nm they showed significant photocytotoxicity. Interestingly, conjugating the parent complex to cell penetrating octaarginine, results in comparable membrane permeability but a wider distribution of the dye within the cytoplasmic region of the cell. It was also nuclear excluding, and there was no evidence for specific localization of $[Ru(bpy)_2phen\text{-}Ar\text{-}Arg_8]^{10+}$ within the mitochondria. Yet, this conjugate was found to be more cytotoxic than the $[(Ru(bpy)_2phen\text{-}Ar)_2\text{-}MPP]^{7+}$ under the same conditions which suggests it is not specifically damage to the mitochondria which is responsible for cytotoxicity/photocytotoxcity of these complexes.

Overall this work highlights the value in combining luminescent metal complexes with the targeting capability of MPPs in directing metal complexes to the mitochondria and

Table 1. Photophysical Data of All Compounds Recorded in PBS (pH 7.4)

compound	Φ (%)	τ (ns) 18 °C aerated	τ (ns) 18 °C deaerated	τ (ns) @ 37 °C aerated	τ (ns) @ 37 °C deaerated
$[Ru(bpy)_2$ phen-Ar-COOH$]^{2+}$	0.046 ± 0.003[b]	455 ± 11	780 ± 9	–	–
$[Ru(bpy)_2phen\text{-}Ar\text{-}Arg_8]^{10+}$	0.067 ± 0.005[b]	579 ± 11	1.02 μs ± 9 ns	–	–
$[(Ru(bpy)_2phen\text{-}Ar)_2\text{-}MPP]^{7+}$	0.053 ± 0.002[a]	698 ± 6	1.23 μs ± 10 ns	458 ± 7	948 ± 6

[a]Standard used $[Ru(bpy)_3]^{2+}$ 0.04 ± 0.002

dx.doi.org/10.1021/ja508043q | J. Am. Chem. Soc. 2014, 136, 15300−15309

confirms overall the value of peptides in targeted imaging by metal complexes. Although toxicity may be an issue over longer times, the probes are potentially powerful tool for short-term dynamic studies of mitochondrial, cellular function both for monitoring of disease progression, and in *in vitro* studies of therapy, e.g., in assessment of mitochondrial effectors.

■ ASSOCIATED CONTENT

Supporting Information

All experimental details and characterization of novel materials, spectra, HPLC traces, and additional biological data. This material is available free of charge via the Internet at http://pubs.acs.org.

■ AUTHOR INFORMATION

Corresponding Author

Tia.Keyes@dcu.ie

Notes

The authors declare no competing financial interest.

■ ACKNOWLEDGMENTS

Based upon works supported by Science Foundation Ireland under [10/IN.1/B3025] and [12/TIDA/B2382]. The National Biophotonics and Imaging Platform, Ireland, was established through funding received by the Irish Government's PRTLI, Cycle 4, and EU Structural Funds Programmes 2007−2013. C.S.B. and T.E.K. gratefully acknowledge the Irish Research Council for PhD scholarship funding. Professor R O'Kennedy, DCU, is gratefully acknowledged for access to cell culture facilities.

■ REFERENCES

(1) Yotter, R. A.; Wilson, D. M. *IEEE Sens. J.* **2004**, *4*, 412.
(2) Li, Z.; Graham, B. H. *Methods Mol. Biol.* **2012**, *837*, 63−72.
(3) Diepart, C.; Verrax, J.; Calderon, P. B.; Feron, O.; Jordan, B. F.; Gallez, B. *Anal. Biochem.* **2010**, *396*, 250−256.
(4) Morris, K. J.; Roach, M. S.; Xu, W.; Demas, J. N.; DeGraff, B. A. *Anal. Chem.* **2007**, *79*, 9310−9314.
(5) Abdel-Shafi, A. A.; Ward, M. D.; Schmidt, R. *Dalton Trans* **2007**, 2517−2527.
(6) Fercher, A.; Borisov, S. M.; Zhdanov, A. V.; Klimant, I.; Papkovsky, D. B. *ACS Nano* **2011**, *7*, 5499−5508.
(7) Vanderkooi, J. M.; Wright, W. W.; Erecinska, M. *Biochemistry* **1990**, *29*, 5332−5338.
(8) Yoshihara, R.; Yamaguchi, T.; Hosaka, Y.; Takeuchi, M.; Tobita, T. S. *Angew. Chem.* **2012**, *51*, 4148−4151.
(9) Zhdanov, A. V.; Dmitriev, R. I.; Papkovsky, D. B. *Cell. Mol. Life Sci.* **2010**, *68*, 903−917.
(10) Dmitriev, R. I.; Papkovsky, D. B. *Cell. Mol. Life Sci.* **2012**, *69*, 2025−2039.
(11) Choi, N. W.; Verbridge, S. S.; Williams, R. M.; Chen, J.; Kim, J. Y.; Schmehl, R.; Farnum, C. E.; Zipfel, W. R.; Fischbach, C.; Stroock, A. D. *Biomaterials* **2012**, *33*, 2710−2722.
(12) Zhang, S.; Hosaka, M.; Yoshihara, T.; Negishi, K.; Iida, Y.; Tobita, S.; Takeuchi, T. *Cancer Res.* **2010**, *70*, 4490−4498.
(13) Korzeniowska, B.; Nooney, R.; Wencel, D.; McDonagh, C. *Nanotechnology* **2013**, *24*, 442002.
(14) Koren, K.; Dmitriev, R. I.; Borisov, S. M.; Papkovsky, D. B.; Klimant, I. *ChemBioChem* **2012**, *13*, 1184−1190.
(15) Baggaley, E.; Botchway, S. W.; Haycock, J. W.; Morris, H.; Sazanovich, I. V.; Williams, J. A. G.; Weinstein, J. A. *Chem. Sci.* **2014**, *5*, 879−886.
(16) Neugeburger, U.; Pellegrin, Y.; Moran, N.; Signac, W.; Forster, R. J.; Keyes, T. E. *Chem. Commun.* **2008**, 5307−5309.
(17) Cosgrave, L.; Neugebauer, U.; Forster, R. J.; Keyes, T. E. *Chem. Commun.* **2010**, *46*, 103−105.
(18) Adamson, K.; Dolan, C.; Moran, N.; Forster, R. J.; Keyes, T. E. *Bioconj. Chem.* **2014**, *25*, 928−944.
(19) Balzani, V., Bergamini, G.; Campagna, S.; Puntoriero, F. *Topics in Current Chemistry, Photochemistry and Photophysics of Coordination Compounds*; Balzani, V., Campagna, S., Eds.; Springer-Verlag: Berlin, 2007; Vol. *280*, pp 1−36.
(20) Dolan, C.; Moriarty, R.; Lestini, E.; Devocelle, M.; Forster, R. J.; Keyes, T. E. *Inorg. Biochem.* **2013**, *119*, 65−74.
(21) Louie, M. W.; Liu, H. W.; Lam, M.H-C.; Lam, Y.-W.; Lo, K.K-W. *Chem.—Eur. J.* **2011**, *17*, 8304−8308.
(22) Jankte, D.; Cokoja, M.; Pothig, A.; Herrmann, W. A.; Kuhn, F. E. *Organometallics* **2013**, *32*, 741−744.
(23) Dobrucki, J.W. *J. Photochem. Photobiol.* **2001**, *127*, 136−144.
(24) Duchen, M. R.; Szabadkai, G. *Essays Biochem.* **2010**, *47*, 115−37.
(25) Tiede, L. M.; Cook, E. A.; Morsey, B.; Fox, H. S. *Cell Death Dis.* **2011**, *2*, e246.
(26) Galluzzi, L.; Larochette, N.; Zamzami, N.; Kroemer, G. *Oncogene* **2006**, *25*, 4812−4830.
(27) Green, K.; Brand, M. D.; Murphy, M.p. *Diabetes* **2004**, *53*, 110−118.
(28) Armstrong, J. S. *J. Pharmacol.* **2007**, *151*, 1154−1165.
(29) Smith, R. A. J.; Porteous, C. M.; Gane, A. M.; Murphy, M. P. *Proc. Natl. Acad. Sci. U. S. A.* **2003**, *100*, 5407−5412.
(30) Horton, K. L.; Stewart, K. M.; Fonseca, S. B.; Guo, Q.; Kelley, S. O. *Chem. Biol.* **2008**, *15*, 375−382.
(31) Carneado-Fernandez, J.; Van Gool, M.; Martos, V.; Castel, S.; Prados, P.; Mendoza, J. D.; Giralt, E. *J. Am. Chem. Soc.* **2005**, *127*, 869−874.
(32) Komor, A. C.; Schneider, C. J.; Weidmann, A. G.; Barton, J. K. *J. Am. Chem. Soc.* **2012**, *134*, 19223−19233.
(33) Chen, T.; Mei, W.-J.; Wong, Y.-S.; Liu, J.; Liu, Y.; Xie, H.-S.; Zheng, W.-J. *Med. Chem. Comm.* **2010**, *1*, 73−75.
(34) Pisani, M. J.; Weber, D. K.; Heimann, K.; Collins, J. G.; Keene, R. F. *Metallomics* **2010**, *2*, 393−396.
(35) Li, P. Y.; Lau, C. T. S.; Louie, M. W.; Lam, Y. W.; Cheng, S. H.; Lo, K. K. W. *Biomaterials* **2013**, *34*, 7519−7532.
(36) Baggaley, E.; Gill, M. R.; Green, N. H.; Turton, D.; Sazanovich, I. V.; Botchway, S. T.; Smythe, C.; Haycock, J. W.; Weinstein, J. A.; Thomas, J. A. *Angew. Chem.* **2014**, *53*, 3367−3371.
(37) Gill, M. R.; Garcia-Lara, J.; Foster, S. J.; Smythe, C.; Battaglia, G.; Thomas, J. A. *Nat. Chem.* **2009**, *1*, 662−667.
(38) McDonnell, U.; Kerchoffs, J. M. C. A.; Castineiras, Rosa P. M.; Hicks, M. R.; Hotze, Anna C. G.; Hannon, M.; Rodger, A. *Dalton Trans.* **2008**, 667−675.
(39) Baggaley, E1; Gill, M. R.; Green, N. H.; Turton, D.; Sazanovich, I. V.; Botchway, S. W.; Smythe, C.; Haycock, J. W.; Weinstein, J. A.; Thomas, J. A. *Angew. Chem., Int. Ed. Engl.* **2014**, *24;53* (13), 3367−71.
(40) Hissler, M.; Connick, W. B.; Geiger, D. K.; McGarrah, J. E.; Lipa, D.; Lachicotte, R. J.; Eisenberg, R. *Inorg. Chem.* **2000**, *39*, 447−457.
(41) Martin, A.; Moriarty, R. D.; Long, C.; Forster, R. J.; Keyes, T. E. *Asian J. Org. Chem.* **2013**, *9*, 763−778.
(42) Van Houten, J.; Watts, R. J. *J. Am. Chem. Soc.* **1976**, *98*, 4853−4858.
(43) Keyes, T. E.; Vos, J. G.; Kolnaar, J. A.; Haasnoot, J.; Reedijk, J.; Hage, R. *Inorg. Chim. Acta* **1996**, *245*, 237−242.
(44) Demas, J. N.; Adamson, A. W. J. *Am. Chem. Soc.* **1973**, *95*, 5159.
(45) Blackmore, L.; Moriarty, R.; Dolan, C.; Adamson, K.; Forster, R. J.; Devocelle, M.; Keyes, T. K. *Chem. Commun.* **2013**, *49*, 5658−2660.
(46) Park, W.-H.; Han, Y.-W.; Kim, S.-K.; Kim, S.-Z. *J. Cell. Biochem.* **2007**, *102*, 98−109.
(47) Chen, Q.; Vazquez, E. D.; Moghaddas, S.; Hoppel, C. L.; Lesnefsky, E. J. *J. Biol. Chem.* **2003**, *38*, 36027−36031.
(48) Drose, S.; Brandt, U. *J. Biol. Chem.* **2008**, *31*, 21649−21654.
(49) Han, Y.-W.; Moon, H.-J.; You, B.-R.; Kim, S.-Z.; Kim, S.-H.; Park, W.-H. *Anticancer Res.* **2009**, *29*, 4423−4432.
(50) Balaban, R. S.; Nemoto, S.; Finkel, T. *Cell* **2005**, *120*, 483−495.

(51) Maguire, J. J.; Kagan, V. E.; Packer, L. *Biochem. Biophys. Res. Commun.* **1992**, *188*, 190−197.
(52) Choi, J. P.; Bard, A. J. *Anal. Chim. Acta* **2005**, *541*, 143−150.